Supplementary Information (SI) for Sustainable Energy & Fuels.

Solar H_2 production by a Perovskite/Silicon tandem cell using urea oxidation

Joudi Dabboussi,[a] Vincent Dorcet,[a] Muriel Escadeillas,[a] Corinne Lagrost,[a,b] Nicolas Penin,[c] Rawa Abdallah,[d] Muriel Matheron,*[e] Gabriel Loget*[f]

[a] Univ Rennes, CNRS, ISCR (Institut des Sciences Chimiques de Rennes)-UMR6226; Rennes, 35000, France.

[b] Univ Rennes CNRS, ScanMAT, UAR 2025, Rennes, 35000, France

[c] Univ. Bordeaux, CNRS, Bordeaux INP, ICMCB, UMR 5026, F-33600 Pessac, France.

[d] Lebanese University, EDST, AZM Center for Research in Biotechnology and Its Applications Laboratory of Applied Biotechnology, LBA3B, El Mitein Street, Tripoli, Lebanon.

[e] Univ. Grenoble Alpes, CEA, LITEN, Campus Ines, 73375 Le Bourget du Lac, France.
*muriel.matheron@cea.fr

[f] University of Bordeaux, Bordeaux INP, ISM, UMR CNRS 5255, Pessac 33607, France.
*gabriel.loget@cnrs.fr

1. Experimental details

1.1. Preparation of the electrodes

The electrocatalysts were synthesized via a simple two-step method involving a hydrothermal process followed by annealing, adapted from the method reported by Yu *et al.*[1] The Ni foams (99.5%, Goodfellow) were first immersed in a 3 M HCl solution (35%, VWR Chemicals) and sonicated for 10 min in acetone (≥99%, VWR Chemicals), ethanol (96°, VWR Chemicals) and ultrapure water (resistivity of 18.2 MΩ cm (Purelab Classic UV)). The anode ($NiMoO_{4\text{-anod}}$) and the cathode ($NiMoO_{4\text{-cathod}}$) were derived from the same precursor foam (consisting in a $NiMoO_4 \cdot xH_2O$ coating deposited on a Ni foam), that were annealed differently. To prepare the precursor foam, a 35 mL solution containing 73 mM $Na_2MoO_4 \cdot 2H_2O$ (98%, Alfa Aesar), 70 mM $Ni(NO_3)_2 \cdot 6H_2O$ (98%, Thermoscientific) was first prepared and stirred for 10 min. When a clear solution was obtained, 30 mL were transferred in a 50 mL PTFE lined reactor that already contained the cleaned Ni foam surface (1.5 x 5 cm²). The complete setup was placed in a stainless-steel autoclave and maintained for 6 hours at 150 °C. After cooling to room temperature, the precursor foam was rinsed with ethanol and water. $NiMoO_{4\text{-anod}}$ was produced by annealing the precursor foam under an Ar atmosphere at 300 °C for 2 h (heating ramp = 5 °C min^{-1}). $NiMoO_{4\text{-cathod}}$ was produced by annealing the precursor foam in an H_2/Ar (5%/95%) atmosphere at 400 °C for 2 h (heating ramp = 5 °C min^{-1}). To make the electrode, a Ni wire was connected to the foam and insulated using hydrophobic tape.

1.2. Characterization

The X-ray diffraction (XRD) measurements were performed in reflection mode on a Bruker D8 Advance diffractometer equipped with a LynxEye fast detector and working with monochromatized Cu Kα1 radiation (λ = 1.5406 Å). Scanning electron microscopy (SEM) was performed using a JSM 7100 F (JEOL). Elemental mapping was performed using Aztec software with the help of an energy dispersive scattering (EDS) detector X-MAXN 80T (Oxford). Scanning transmission electron microscopy (STEM) was performed using a JEOL JEM 2100 LaB_6 microscope working at 200 kV. The images were taken in bright field mode using the GATAN Orius 200D Camera. The same camera was used to acquire the diffraction patterns. Elemental mapping was performed using Aztec software with the help of an energy dispersive scattering (EDS) detector X-MAX^N 80T (Oxford).

XPS data have been collected by a NEXSA G2 (ThermoFischer Scientific) spectrometer using the Al Kα X-ray source working at 1486.6 eV and using a spot size of 200 µm². Survey spectra (0-1000 eV) were acquired with an analyzer pass energy of 200 eV (1 eV/step); high-resolution spectra used a pass energy of 50 eV (0.1 eV/step). Peaks were referenced to C 1s photoelectron peak energy at 284.8 eV. The peak areas were normalized by the manufacturer-supplied sensitivity factor (S_{C1s} = 1, S_{Ni2p} = 20.765,

S_{Mo3d} = 11.008). For each sample, XPS survey spectra were recorded at three different locations and we did not see any significant difference. Curve-fittings were performed with CasaXPS version 2.3.26, using a Shirley background for Mo 3d.

1.3. Preparation of the PK/Si PV cells

Silicon bottom cell fabrication. Silicon heterojunction bottom cells were processed starting from commercially available n-type float-zone (100) oriented both side polished silicon wafers (chemical mechanical polishing), 4-inch size, with a thickness between 260 and 300 µm and a resistivity between 1 and 5 Ω·cm. A wet cleaning with hydrofluoric acid (HF) and hydrochloric acid (HCl) was performed to remove native oxide and contaminants, before the deposition of intrinsic amorphous silicon layers (a few nanometers thick) on both sides of the wafer, by plasma-enhanced chemical vapor deposition (PECVD) at 200 °C with SiH_4 and H_2 gases. Doped amorphous silicon layers were then deposited by PECVD on each side of the wafer, adding phosphine gas (PH_3) for the n-doped a-Si:H layer and diborane (B_2H_6) for the p-doped a-Si:H. The back-side electrode, made of indium tin oxide (ITO), was then deposited by sputtering. The recombination layer, also made of ITO, was then deposited by physical vapor deposition (PVD).

Perovskite top cell fabrication. Silicon heterojunction bottom cell wafers were laser cut to 5×5 cm² size. A layer of 200 nm silver was then thermally evaporated to form the back-side electrode. Perovskite formulation was prepared in a glovebox the day before deposition, as follows. The formamidinium lead iodide ($FAPbI_3$), lead bromide ($PbBr_2$) and cesium iodide (CsI) mother solutions are prepared by dissolving lead iodide (PbI_2) and formamidinium iodide (FAI) in a N,N-dimethylformamide/dimethylsulfoxide mixture (DMF/DMSO) at 40 °C, $PbBr_2$ in DMF/DMSO mixture at 40 °C and CsI in DMSO at ambient temperature. The solution of $Cs_xFA_{1-x}Pb(I_1\text{-}yBr_y)_3$ was prepared the next day, mixing in a vial the $FAPbI_3$, $PbBr_2$ and CsI solutions so that x = 0.15 and y = 0.17. Right before the top cell fabrication, a 30 min UV-ozone surface treatment was applied to the recombination ITO. Cells were immediately introduced into the glovebox to perform further steps under inert nitrogen atmosphere. The hole transport layer (HTL) was prepared from commercially available 2-PACz ([2-(9H-carbazol-9-yl)ethyl]phosphonic acid) dissolved into ethanol. The 2-PACz solution was spin-coated on the recombination ITO, followed by annealing at 100 °C for 10 min on a hot plate. The perovskite layer was then deposited by spin-coating, with a chlorobenzene quenching step to promote perovskite crystallization. Annealing was performed on a hot plate at 100 °C for 1 h. The electron transport layer (ETL) was then formed on top of the perovskite by evaporation of C60 and BCP (bathocuproine). The transparent front side electrode was obtained by sputtering at ambient temperature to form a 100 nm thick ITO layer. A 200 nm thick gold grid, thermally evaporated, was finally added. A conductive metal

ribbon (3M 3007 solar tape) was then manually pressed on the solar cells front- and backsides. Cells were stored in the dark and in nitrogen before use.

1.4. Power conversion efficiency measurements

A class A solar simulator (Oriel 92190, Xe source and AM1.5 filter) is used to simulate 1 sun illumination. Calibration is performed with a standard silicon solar cell (monocrystalline silicon solar cell, WPVS) from Fraunhofer ISE and a spectrophotometer (Aescusoft). Crocodile clamps are placed on the metal ribbons and current-bias i(V) curves of the solar cells are recorded using a Keithley 2602A source measure unit (SMU). A circular 3.2 cm² mask is used to define the illuminated area (A_{PV} = 3.2 cm²). Results presented here are not corrected for the shading losses due to metal contacts. Acquisitions are monitored with a homemade Labview software. Several i-V sweeps are performed under continuous illumination until the efficiency stabilizes, under the following conditions: reverse scans (from 2.2 V to – 1.5 V), one scan every 10 s, steps: 50 mV, dwell time: 20 ms, scan speed: 1.36 V·s^{-1}, number of power line cycles (NPLC) set to 1, cell kept at open circuit between measurements.

1.5. Electrochemical and photoelectrochemical measurements

The electrochemical measurements were performed with a Zennium potentiostat (Zahner). The electrolyte was a 1 M KOH (99.9%, Fisher Scientific) aqueous solution. For three-electrode measurements, a carbon electrode was used as a counter electrode and a Hg/HgO (1 M KOH) was employed as the reference electrode. The light was supplied by a solar simulator (LS0106, LOT Quantum Design) equipped with an AM 1.5G filter. The power intensity of the light source, where the photoanode was located, was adjusted to 100 mW cm^{-2} using an ILT1400 radiometer (International Light Technologies). The potentials versus Hg/HgO were converted into potentials versus reversible hydrogen electrode (RHE) using the following relationship: $E_{RHE} = E_{Hg/HgO} + 0.098 + 0.059$ pH. A 2-compartment cell was used to detect the gas while using a two-electrode setup in 0.33 M urea in 1 M KOH. The composition of the gas phase during electrolysis using the $NiMoO_{4\text{-anod}}$ anode and the $NiMoO_{4\text{-cathod}}$ cathode was measured by using a micro-GC Agilent 990 instrument equipped with a TCD detector at a constant current density of 3 mA cm^{-2} in a two-compartment cell with the anolyte and the catholyte separated by a Zirfon® diaphragm. Faradaic efficiencies were calculated as follows:

$$\eta = \frac{n\ experimental}{n\ theorical}$$

$$n\ theoretical = \frac{I * t}{96500 * n_{charge}}$$

$$n = \frac{P * V}{R * T}$$

With η, P, R, T and n_{charge} being the faradaic efficiency, pressure, gas constant and stoichiometric charge number respectively.

The 2-electrodes setup electrical measurements were performed using a potentiostat as a passive measurement tool, these measurements were verified by a multimeter.

1.6. Ion analysis in the solution

The quantification of NO_2^- was conducted using ion chromatography (model 881 Compact IC Pro, Metrohm) with a conductivity detector. The chromatographic column employed was a Metrosep A supp 16 – 250/4.0, maintained at a temperature of 45 °C. The eluent used for the chromatographic separation consists of 3.75 mM Na_2CO_3 and 0.375 mM NaOH, with a flow rate of 0.8 mL/min. All samples were diluted by 200 and analyzed the same day, directly after electrolysis. Ni and Mo ions quantification was performed by a Thermo Scientific iCAP 7000 series ICP-AES spectrometer. Faradaic efficiency of nitrite was calculated as follow:

$$\eta = \frac{n\ experimental}{n\ theorical}$$

$$n\ theoretical = \frac{I\ *\ t}{96500 *\ n_{charge}}$$

$$n\ experimental = \frac{C\ (mg/L) * V\ (L)}{M}$$

1.7. Efficiency calculations

Generally, solar-to-H_2 efficiency (η_{STH}) is defined as follows:

$$\eta_{STH}(\%) = \frac{j_{op} \times E^{0}_{cell} \times \eta_{F,H2}}{P_{sun}} \times 100 \quad \textbf{(1)}$$

with j_{op} being the operating current (here, 33.4 x10^{-3} A), E^{0}_{cell} the cell potential required to generate H_2, $\eta_{F,H2}$ the Faradaic efficiency for H_2 (here, 1) and P_{sun} the illumination power (0.32 W). E^{0}_{cell} is calculated using the Gibbs energy of the reaction and is typically 1.23 V for conventional water splitting.

In our case, the oxidation process involves UOR and not OER. Therefore, different E^{0}_{cell} values should be used to calculate η_{STH}. E^{0}_{cell} values are reported in Table S1.[2]

Table S1. Value of $E^{0}_{cell}$for the different anodic reactions involved in the H_2 production process, data taken from.[2]

	Half-reaction	E^{0}_{cell}
OER	$2\ OH^-(aq) \rightarrow ½\ O_2(g) + H_2O(l) + 2\ e^-$	1.23 V
UOR Sustainable pathway	$(NH_2)_2CO(aq) + 8\ OH^-(aq) \rightarrow N_2(g) + 6\ H_2O(l) + CO_3^{2-}(aq) + 6\ e^-$	0.07 V
UOR Overoxidation pathway	$(NH_2)_2CO(aq) + 16\ OH^-(aq) \rightarrow 2\ NO_2^-(aq) + 10\ H_2O(l) + CO_3^{2-}(aq) + 12\ e^-$	0.77 V

Another method for determining η_{STH}, which has been recently reported,[3] involves the use of Equation (2).

$$\eta_{STH}(\%) = \frac{j_{op} \times E_{PV} \times \eta_{F,H2}}{P_{sun}} \times 100 \quad \textbf{(2)}$$

With E_{PV} being the potential difference generated by the PV cell (here, 1.29 V, see Figure 4b).

In Table S2, we report the values of η_{STH} determined with various methods, including a E^{0}_{cell} value of 1.23 V. This η_{STH} value is erroneous but it is given as a comparative information only, as several works have used this metric in the frame of UOR.

Table S2. η_{STH} values calculated with different methods and different E^{0}_{cell} and E_{PV} values.

Description	**Equation used**	E^{0}_{cell} **(V)**	E_{PV} **(V)**	η_{STH} **(%)**
water splitting	1	1.23	-	12.8
only sustainable pathway	1	0.07	-	0.7
only overoxidation pathway	1	0.77	-	8.0
weighting using the determined Faradaic efficiencies $\eta_{NO_2^-}$ and η_{N2} (Figure 3b)	1	0.07×0.25 + 0.77×0.75	-	6.2
only electrics	2	-	1.29	13.5

2. Supplementary figures

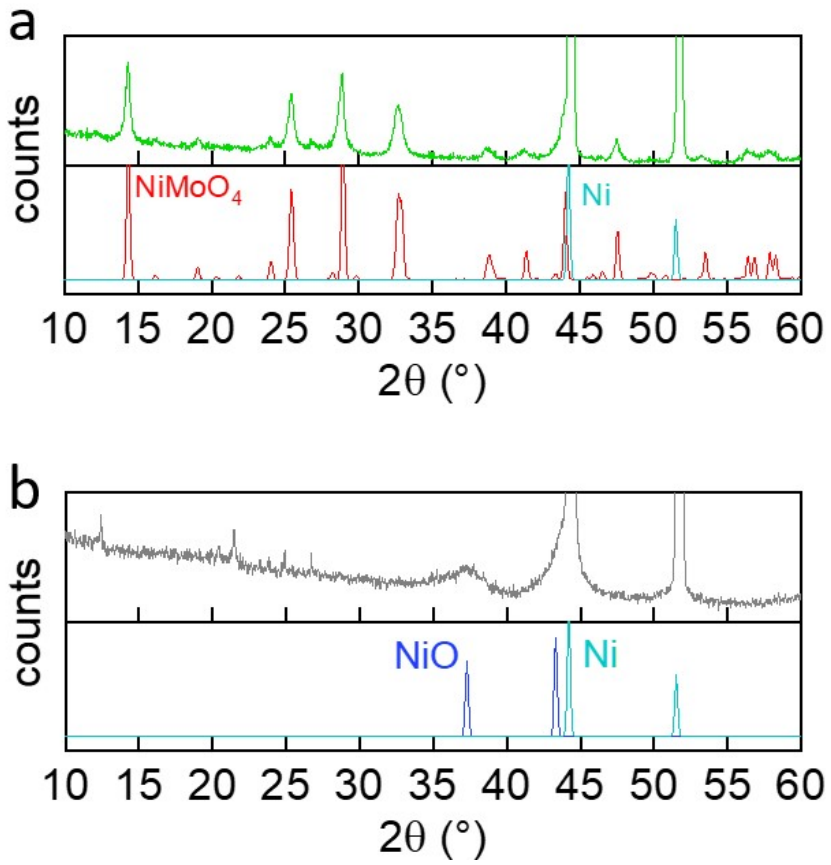

Figure S1. Experimental XRD patterns (top row) recorded for $NiMoO_{4\text{-anod}}$ (a) and $NiMoO_{4\text{-cathod}}$ (b) and theoretical XRD patterns (bottom row) for $NiMoO_4$ (red curve ICCD 00-033-0948), Ni (cyan curve, ICCD 00-004-0850) and NiO (dark blue curve, ICCD 00-044-1159).

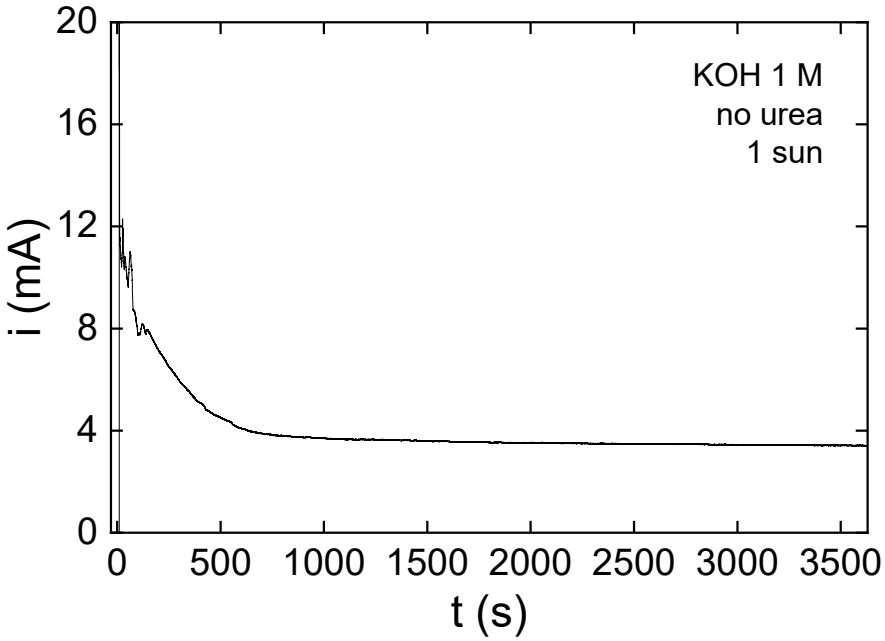

Figure S2. i-t curve of the coupled PK/Si PV cell with the $NiMoO_{4\text{-anod}}$/$NiMoO_{4\text{-cathod}}$ electrochemical system without urea under 1 sun illumination.

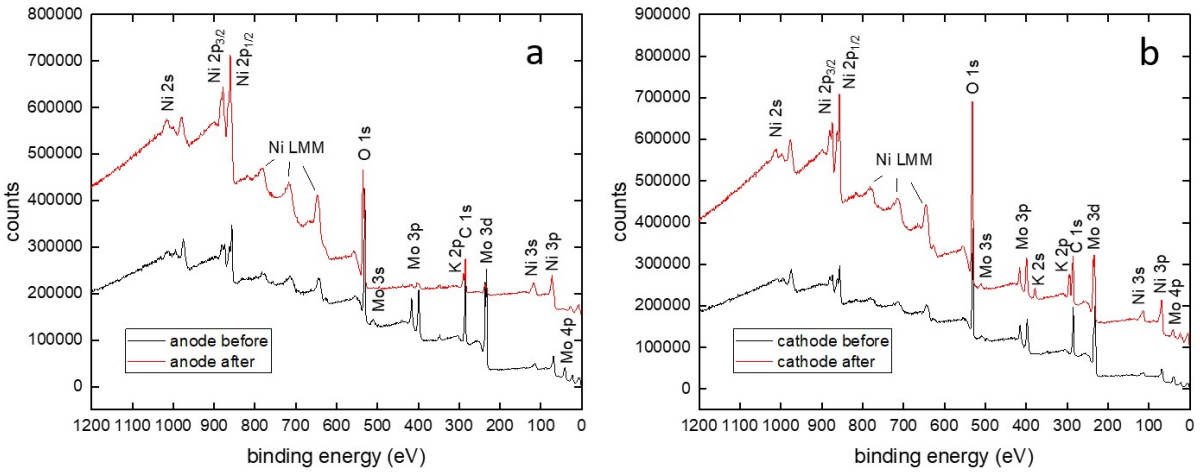

Figure S3. XPS survey spectra of a) $NiMoO_{4\text{-anod}}$ b) $NiMoO_{4\text{-cathod}}$ after synthesis (black spectra) and after 48 h of electrolysis (red spectra).

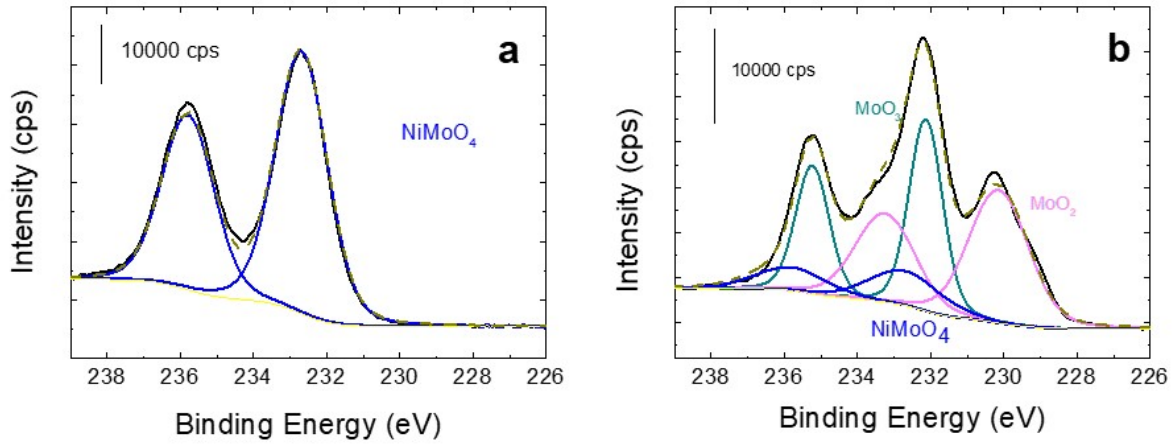

Figure S4. Peak fitted core level spectra in the Mo 3d region of a) $NiMoO_{4\text{-anod}}$ b) $NiMoO_{4\text{-cathod}}$, before electrocatalysis.

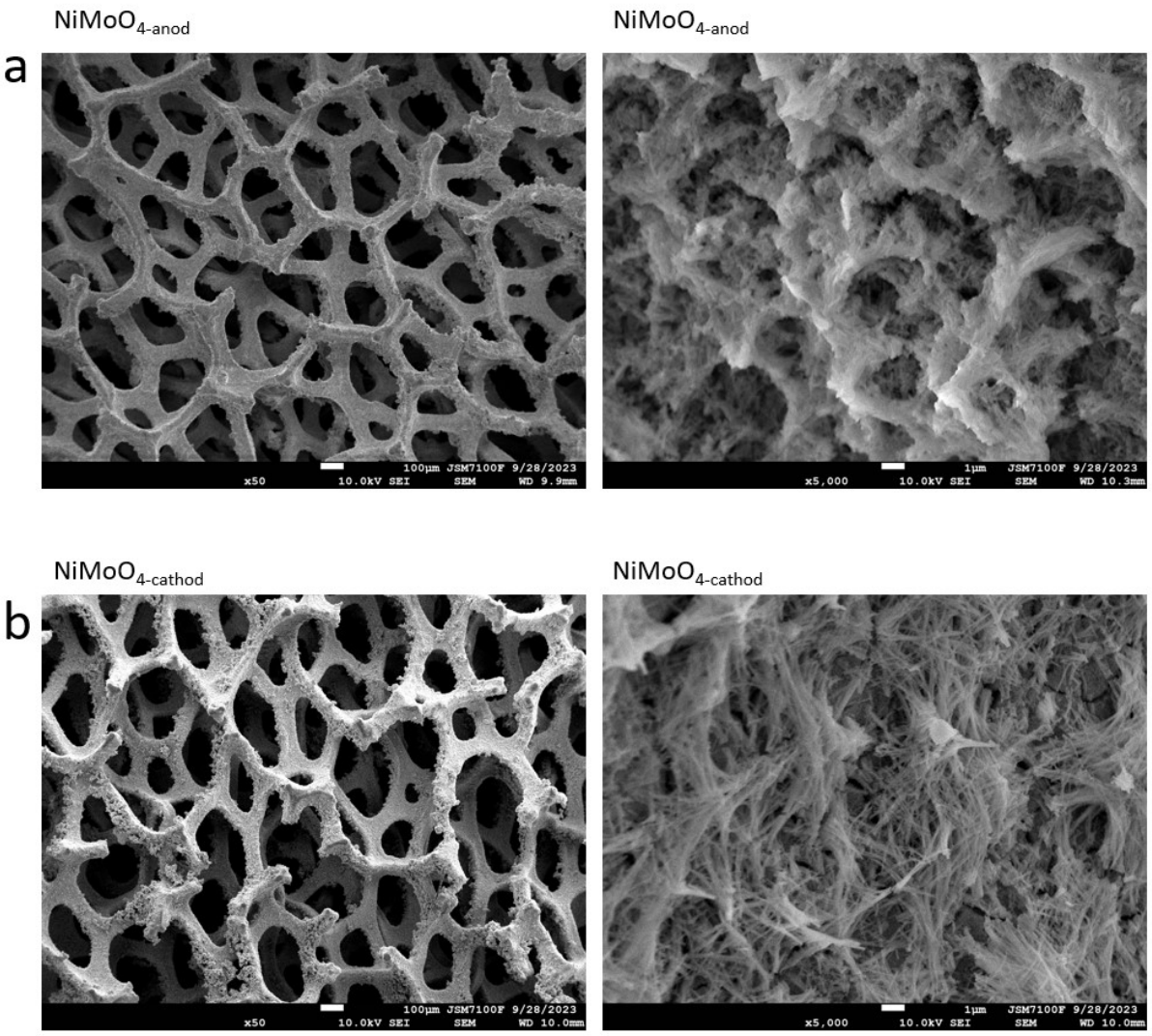

Figure S5. SEM pictures of a) $NiMoO_{4\text{-anod}}$ b) $NiMoO_{4\text{-cathod}}$ after 48h of electrocatalysis.

3. References

(1) Yu, Z.-Y.; Lang, C.-C.; Gao, M.-R.; Chen, Y.; Fu, Q.-Q.; Duan, Y.; Yu, S.-H. Ni–Mo–O Nanorod-Derived Composite Catalysts for Efficient Alkaline Water-to-Hydrogen Conversion via Urea Electrolysis. *Energy Environ Sci* **2018**, *11* (7), 1890–1897. https://doi.org/10.1039/C8EE00521D.

(2) Tatarchuk, S. W.; Medvedev, J. J.; Li, F.; Tobolovskaya, Y.; Klinkova, A. Nickel-Catalyzed Urea Electrolysis: From Nitrite and Cyanate as Major Products to Nitrogen Evolution. *Angew Chem Int Ed* **2022**, *61* (39), e202209839. https://doi.org/https://doi.org/10.1002/anie.202209839.

(3) Zhan, G.; Hu, L.; Li, H.; Dai, J.; Zhao, L.; Zheng, Q.; Zou, X.; Shi, Y.; Wang, J.; Hou, W.; Yao, Y.; Zhang, L. Highly Selective Urea Electrooxidation Coupled with Efficient Hydrogen Evolution. *Nat Commun* **2024**, *15* (1), 5918. https://doi.org/10.1038/s41467-024-50343-8.